An Investigation of Pitting Behavior of Iron-Molybdenum Binary Alloys*

D. A. STOUT*, J. B. LUMSDEN** and R. W. STAEHLE***

Abstract

An investigation of the iron-molybdenum binary system was undertaken to determine the effects of molybdenum on pitting and passive film behavior. Polarization curves, galvanostatically determined pitting potentials, and AES and ESCA surface analysis were employed to investigate binaries in the composition range of 5 to 95% Mo. Passive films, which were formed in a borate buffer solution, were depleted in molybdenum and were in general less protective than that on Fe. Alloying up to 15% Mo increased the resistance to pitting in a borate buffer solution +0.1N KCl solution, but with less effect than observed for stainless steels. Also, the pitting resistance was observed to decrease with increasing temperature for each binary. Precipitated material identified as $FeMoO_4$ was found in the pits and along the flow paths establishing the existence of a salt film containing molybdenum as a factor in the pitting behavior of molybdenum containing alloys.

The addition of small amounts of molybdenum to stainless steels has long been recognized as important in improving the resistance of these alloys to localized corrosion. Bond, *et al*,[1-5] have extensively investigated the effects of molybdenum in ferritic stainless steels varying the percentage of molybdenum, temperature, aging, etc. Austenitic stainless steels with molybdenum additions have also been studied in chloride solutions with the beneficial effects of molybdenum being clearly demonstrated.[6-11] The fact that the percentage of chromium present in these alloys strongly influences the effectiveness of molybdenum, tends to complicate the assessment of the role of molybdenum in improving the resistance to localized corrosion. In order to study the influence of molybdenum on passive film behavior, and its effect on pitting resistance without the presence of chromium, a series of iron-molybdenum binary alloys were investigated.

Experimental

The iron-molybdenum binaries used in this study were prepared by Climax Molybdenum Co. and had a composition of 0, 5, 15, 25, 85, 95, and 100 Wt% molybdenum. The analyses of the Fe and Mo chips used to fabricate the binaries are listed in Table 1. The 0, 5, and 15% Mo alloys were melted, cast in vacuum, and extruded at 2000 F with approximately a 9 to 1 reduction in area to form 1 by 12 inch rods. The rods were annealed in hydrogen for 1 hour and then water quenched. The annealing temperatures were 2200 F for the 0 and 5% Mo alloys, and 1800 F for the 15% Mo alloy. The higher molybdenum containing binaries were formed as arc-melted buttons under one half atmosphere argon. The buttons were inverted and remelted at least twice. They were quenched to room temperature in approximately 1 minute.

The 0, 5, 15, and 100% Mo binaries were machined into one quarter inch diameter cylinders and mounted in Bakelite. The 25, 85, and 95% Mo binaries were too brittle to be machined but could be rough cut using a silicon carbide wheel. These alloys were also mounted in Bakelite and had exposed surface areas approximately equal to the machined samples. The binaries were polished with a series of silicon carbide papers followed by 6 and 1 micron diamond paste. The surfaces were then cleaned with a mild detergent and rinsed with distilled water and methanol. Epoxy or glyptol was applied to the interface between the Bakelite and the sample to prevent crevice corrosion.

The microstructures of the binaries were also investigated. Acid ferric chloride or 10% Nital were used as etchants with the Nital usually giving the best results. The microstructures for these alloys were virtually identical to photomicrographs given by Sykes.[12] Sykes found that with water quenching, binaries with up to 24% Mo could be formed as solid solutions but that second phase material could not be avoided at higher molybdenum contents. The 5 and 15% binaries for this work exhibited no evidence of second phase material, while the Fe25Mo alloy had the needle-like structure that Sykes identified as second phase material. In a more recent study, Sinha,[13] using X-ray diffraction, reported three distinct phase regions for the Fe25Mo alloy. The regions can not be distinguished by their microstructures, but the heat treatment should place the binary in the $\alpha + R$ region where the second phase region (R) contains approximately 50% Mo. The Fe85Mo alloy has second phase material similar to the Fe25Mo alloy but surrounded by a molybdenum rich solid solution. The Fe95Mo alloy appears to be a single phase alloy.

The electrochemical measurements were made in a 0.15N boric acid and 0.15N sodium borate buffer solution with and without the addition of 0.1N postassium chloride. The solutions were adjusted to a pH of 8.4. The experiments were conducted in a pyrex cell with a platinum counter electrode. A saturated calomel electrode was used as the reference electrode connected through a luggin capillary into the cell. The solutions were deaerated with helium for at least 12 hours before any experiments. Temperatures were adjusted by a flowing ethylene glycol temperature control unit.

AES analysis of the binaries were conducted using a Physical Electronics Model 545 scanning Auger microprobe. A 3kV beam voltage was used. The experimental samples with the Bakelite mounts removed were placed in the spectrometer, and the system was evacuated to the 10^{-10} torr range. Depth profiling of the

*Submitted for publication December, 1977; revised September, 1978.

*National Standard Company, Niles, Michigan.

**Rockwell International Science Center, Thousand Oaks, California.

***Ohio State University, Columbus, Ohio.

0010-9312/79/000047/$3.00/0

TABLE 1 — Analysis of Fe and Mo Chips

	Fe	Mo	Cr	C	N	Si	P	Mn	Cu	Al	Ni	Co	S	V
Fe Chips	Bal.	0.005	0.002	0.001	0.004	0.003	0.002	0.003	0.004	0.002	0.062	0.007	0.002	<0.003
Mo Chips	0.040	Bal.	0.071	0.002		0.007		<0.001	<0.001	<0.001	0.007			

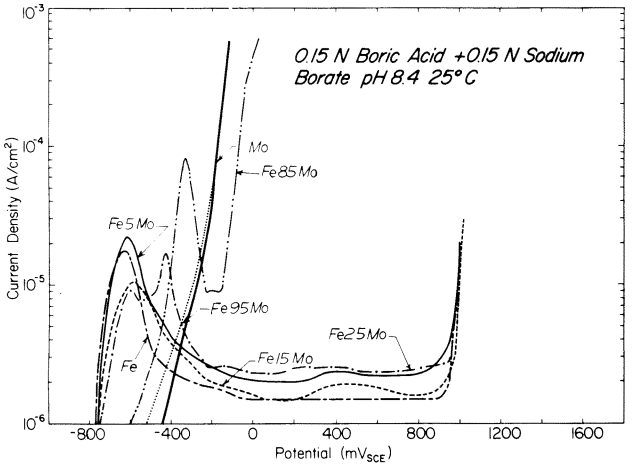

FIGURE 1 — Polarization curves in borate buffer without chloride.

surfaces was conducted using Xenon ions with an accelerating potential of 600 volts at a pressure of 5×10^{-5} torr.

The Physical Electronics Model 548 ESCA-Auger spectrometer was used for the ESCA analysis of the surfaces. The specimens were irradiated with Mg $K\alpha_{1,2}$ (1254 eV) radiation with an applied voltage and current of 10KV and 40 mA. The high resolution ESCA spectra were signal averaged using a Nova 800 microprocessor. All spectra were calibrated using the Au $4f_{7/2}$ standard. The vacuum and sputtering conditions were similar to the Auger analysis.

Results

Polarization Measurements

The polarization curves in the borate solution are shown in Figure 1. Examination of these curves reveal that for up to 15% Mo the polarization behavior is not unlike iron. These alloys have the same open circuit rest potentials, similar passive current densities, and similar transpassive behaviors. The active peaks have a tendency to shift in the noble direction with increasing molybdenum. The Fe25Mo has a double active peak which is characteristic of a two phase material. The passive and transpassive behavior are still similar to iron, but the current densities are elevated in the passive region. A single active peak is observed for the Fe85Mo alloy. The α solid solution behavior for iron is no longer seen for this alloy. A short passive region is followed by molybdenum controlling transpassive behavior. The Fe95Mo binary follows molybdenum controlled behavior. Increasing the percentage of molybdenum over 25% shifts the open circuit corrosion potential in the noble direction.

The addition of chloride to the borate buffer solution modified the polarization curves in several respects. Pitting eliminated much of the passive region for the 0 to 25% Mo alloys, and the current densities in the passive region were higher and increased with temperature. In addition, the presence of chloride and increasing temperature tended to increase the anodic current densities. The open circuit potentials and primary passivation potentials were largely unaffected by chloride or temperature changes.

Pitting Potential Measurements

Potentiodynamic techniques did not result in accurate pitting potentials for these alloys because of the long induction times

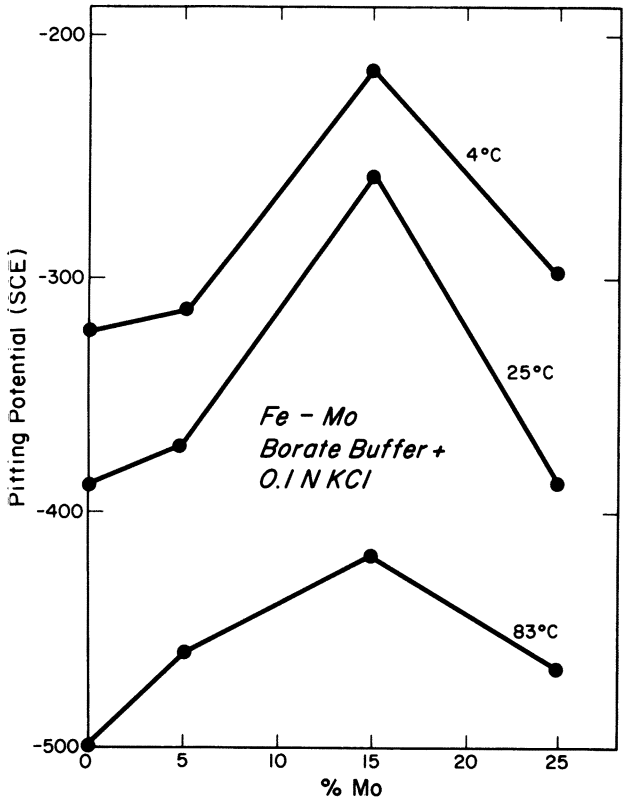

FIGURE 2 — Pitting potential (SCE) versus %Mo for 4, 25, and 85 C.

required for the initiation of pitting. The galvanostatic technique was used to determine the pitting potentials for the 0 to 25% Mo alloys.[14] Constant current densities were applied to the samples and the potential changes were monitored. Three different current densities were used for each alloy at each temperature with the potentials for the different current densities converging at the pitting potential. The pitting potentials as functions of molybdenum content and temperature are given in Figure 2. At any of the three temperatures investigated, increasing the percentage of molybdenum in the alloy shifts the pitting potential in the noble direction. Alloying up to 5% Mo has little effect on the pitting potential, while increasing to 15% Mo causes a large change. Above 15% Mo the pitting potential shifts back in the active direction. This folding back of the potential for the Fe25Mo alloy can be attributed to the two phase structure. At any given molybdenum content an increase in temperature shifts the pitting potential in the active direction and decreases the resistance to pitting attack. The largest decrease in the pitting potential occurs for the Fe15Mo alloy, indicating that temperature has a greater effect on alloys with large molybdenum content.

AES Results

The passive films in the borate buffer solution for the alloys with 0 to 85% Mo were investigated. Sputter profiles of these films revealed that there was no detectable molybdenum on the surface of the oxide films for the binaries up to 15% Mo, while small amounts of molybdenum were found on the surface for the Fe25Mo and Fe85Mo binaries. Figure 3 illustrates these results for the Fe85Mo

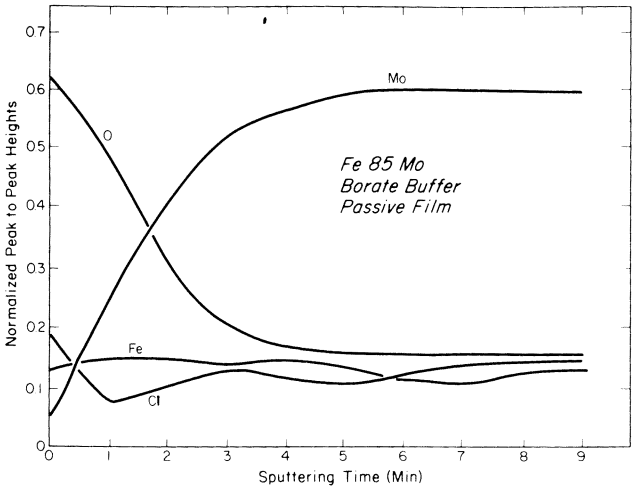

FIGURE 3 – Auger depth profile analysis of Fe85Mo passive film without chloride. (-200 mV).

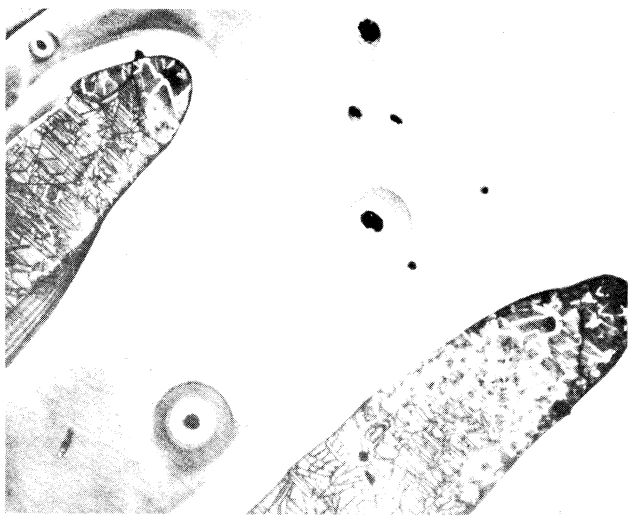

FIGURE 4 – Photomicrograph of pitted Fe15Mo surface. 41X

binary. The Auger intensities are calculated by measuring the peak-to-peak heights for the Mo (221 eV), Fe (703 eV), O (510 eV), and C (272 eV) transitions. The peak heights are normalized by dividing each transition by the sum of the peak heights for all of the measured transitions. This results in the sum of all the normalized peak-to-peak heights equalling one at all times during sputtering. This procedure tends to compensate for any drifts in the electron beam energy or analyzer sensitivity during the profile measurements. The molybdenum is depleted in the surface layers of the film with the concentration increasing towards the substrate. This behavior was observed for all of the binaries investigated.

The composition of the pitted surface of the Fe15Mo alloy after exposure to the borate buffer plus chloride solution was also investigated by Auger analysis. In order to understand the Auger results, a detailed description of the pit morphology is first needed. The pits were formed at a potential approximately 300 mV above the pitting potential. Initially, the sample was passivated with low current densities. However, breakdown of the passive film occurred within a short period. A small dark stain appeared on the surface followed by the formation of a pit as the current increased. Usually two or three primary pits formed on a sample area of 0.3 cm^2. Corrosion product spilled from the pits and flowed across the surface of the sample. While this occurred, secondary pits formed outside the flow regions but were rapidly engulfed by the flowing corrosion product. Figure 4 is a photomicrograph of a sample held in a vertical position. Corrosion product flowed vertically down the surface of the sample (which for Figure 4 is toward the bottom left of the figure). For horizontal samples, the flow patterns were concentric and also rapidly covered the surface. Detailed observations of the pit morphology revealed several distinct features. After the corrosion product began to flow from the primary pits, the main area of attack spread out three or four pit diameters from the center of the pits. In the pits and down the flow region, there was an area where considerable material was deposited. The white lines in Figure 4 are cracks in this deposited material. Further down the flow region, there was a very fine line structure that was composed of secondary pits, deposited material, and grain boundary etching. The final region, not shown in Figure 4, has only the evident etching of grain boundaries. The flow region was brightly colored with areas of brown, blue, gold, and green colors. Most of this was due to interference colors of the thin films, while some may have been due to characteristic colors of the oxides of iron and molybdenum. The secondary pits outside the flow regions were irregular in shape, had some concentric coloring around them, but did not have any flow patterns.

Scanning Auger micrographs were taken of the pitted region in order to determine the spatial distribution of the elements. Figure 5a is an absorbed current micrograph of a primary pit with a flow path. The pit formed near the edge of the flat circular surface, and material flowed vertically down towards the bottom of the picture. The central dark area is the primary pit and its flow region. Figures 5b through 5f are Auger images on the initial unsputtered surface for the distribution of K, Cl, Fe, B, O, and Mo, respectively. Cl and K tended to concentrate in the pit and near the flow region as shown in Figures 5b and 5c. The Fe distribution is uniform, except in the flow areas where Cl and K were concentrated, as seen in Figure 5d. B and O were less uniformly distributed. An area of B and O concentration can be seen to the left of the flow path in Figure 5e and 5f, in the probable form of a borate. The molybdenum concentration on the initial surface was too small to be imaged, however after sputtering for several minutes to remove the outer layer of salt, molybdenum could be imaged as shown in Figure 5g. Once the outer layer of potassium and chloride as well as the borate was removed, molybdenum was found to be concentrated in the pit and flow region.

Auger images give the relative concentrations of each element on the surface but cannot accurately describe the concentration differences between the elements at any particular point. The sample surfaces were also depth profiled by means of Xenon ion sputtering, and the results for the different regions are shown in Figures 6 through 9. The Auger results for the unattacked surface are shown in Figure 6. Mo was depleted in the outer layers of the film, while B, K, and Cl extended to the substrate. The films below the pitting potential were similar to the films on the unattacked region shown in Figure 6 but appear to be thinner. Figure 7 illustrates the results for the flow region. The outermost layers had rapid fluctuations in Fe, Mo, and O content, while the K and C dropped to low values. Cl and B were not large and rapidly decreased. After approximately 30 minutes of sputtering, the Fe peak-to-peak ratio dropped, and the Mo increased. Most of the film was characterized by moderate Fe, Mo larger than the substrate value, and high O. Sputtering into the substrate region decreased the Mo and O, while increasing the Fe intensities. These results were almost identical with data for the primary pit wall, with the exception of stronger K and Cl in the pits. The Auger results for the secondary pits exhibited varying results from pit-to-pit, as shown in Figures 8 and 9. In Figure 8, the Mo concentration was small with larger Fe, K, and Cl, while in Figure 9 the Mo intensity was much larger and the K and Cl were reduced. Scanning Auger analysis revealed a halo of K around the secondary pits on the outside surfaces extending approximately one pit diameter.

ESCA Results

The results for the ESCA analysis of the deposited material are shown in Figure 10. The Fe 2p transition in Figure 10a occurred at 709.8 eV with a satellite transition at 715 eV. The appearance of a

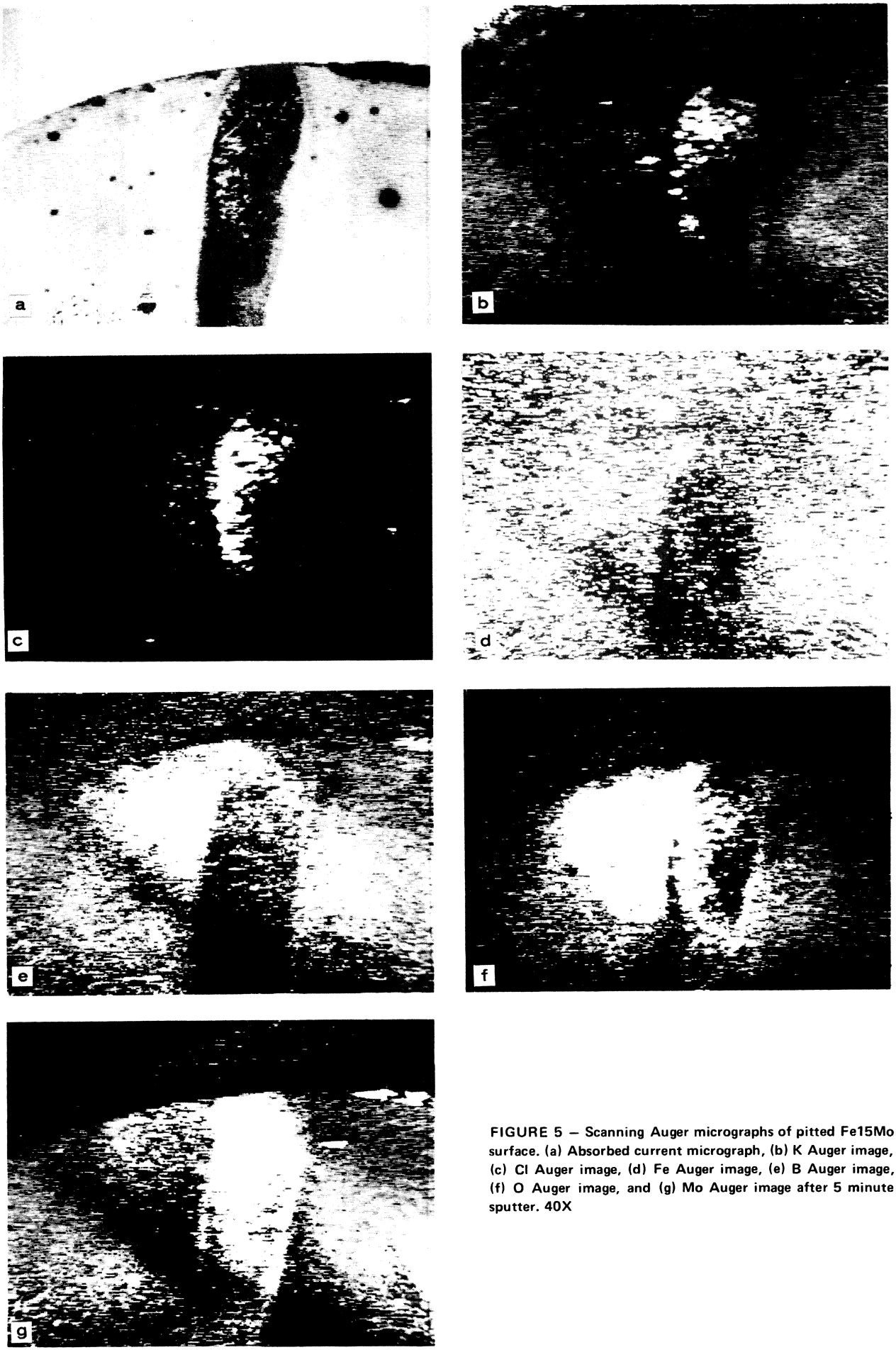

FIGURE 5 – Scanning Auger micrographs of pitted Fe15Mo surface. (a) Absorbed current micrograph, (b) K Auger image, (c) Cl Auger image, (d) Fe Auger image, (e) B Auger image, (f) O Auger image, and (g) Mo Auger image after 5 minute sputter. 40X

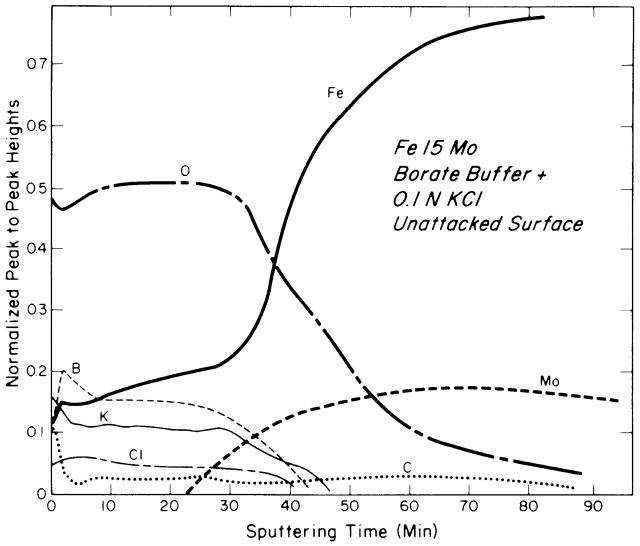

FIGURE 6 — Auger depth profile analysis of the unattacked surface above the pitting potential.

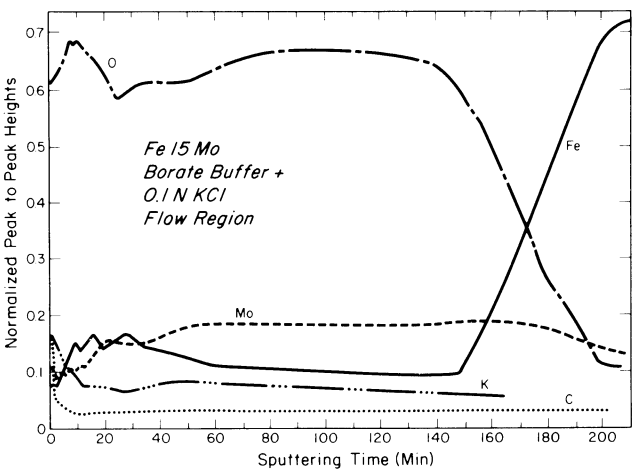

FIGURE 7 — Auger depth profile analysis of the pit flow region containing precipitated material.

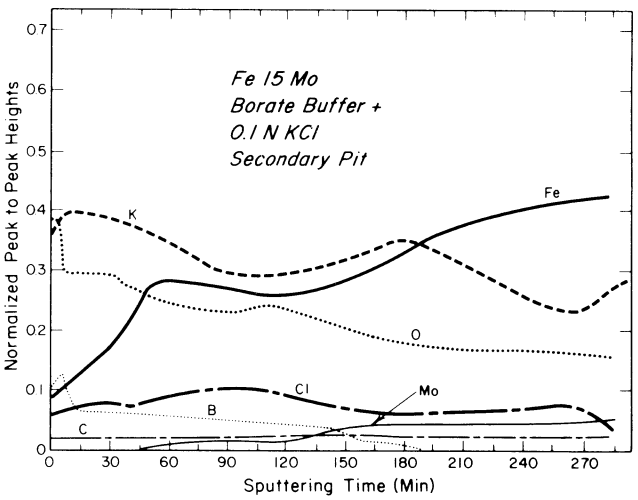

FIGURE 8 — Auger depth profile analysis of a secondary pit with small molybdenum.

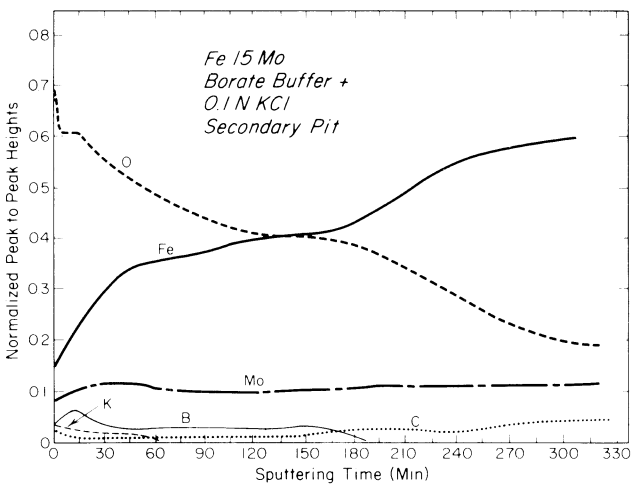

FIGURE 9 — Auger depth profile analysis of a secondary pit with moderate molybdenum.

satellite transition at 715 eV can be associated with iron in the +2 oxidation state.[15] The Mo 3d transitions in Figure 10b appeared at 235.5 eV and 232.5 eV. These energies correspond to molybdenum in the +6 oxidation state. There was no evidence of metallic molybdenum or molybdenum in any of the lower oxidation states.

The passive film below the pitting potential was also studied, with the results that molybdenum transitions were found for the +6 oxidation state and for metallic molybdenum. The Fe 2p spectra also had a small shoulder which originated from metallic iron. The presence of the metallic lines indicates that the thickness of the film is less than the escape depth of the photoelectrons, *i.e.*, a few tens of Angstroms.

Sputtering of these films produces partial reduction of the iron[15] and the molybdenum[16] to the metallic state, resulting in an ESCA spectrum with both oxidized and metallic lines. The ESCA spectra of the inner layers of these films are therefore affected by the sputtering process and are not representative of the oxidation states found below the original surfaces. Under these circumstances, valid chemical information is available for only the unsputtered condition.

Discussion

The electrochemical response of the alloys without second phase material (*i.e.*, with 5 and 15% Mo) exposed to the borate buffer solution is very similar to that of iron. The passive current density increases a few microamperes as the molybdenum is increased, and there is a slight broadening of the active peak. In contrast to this, in a sulfate solution at a comparable pH, the addition of molybdenum is more noticeable.[17] In this solution, Fe-15Mo has a significantly larger passive current density and a several hundred millivolt decrease in the extent of the passive zone relative to Fe. In both environments, the transpassive behavior of Mo donimates the electrochemical response of the high Mo binaries.

The pitting potential results can be compared with the work by Bond[2] on 18% Cr ferritic stainless steel with 0 to 4% Mo. Bond found a similar dependence on molybdenum content and temperature as is shown in Figure 2. It was also observed that for the 4.7% Mo steel, the pitting potential began to shift back to lower potentials in a way similar to the Fe25Mo binary. Both cases can be explained by the formation of a second phase that may be itself more susceptible to pitting attack or possibly the second phase and solid solution interface is preferentially pitted. With chromium present, much less molybdenum is needed for a noticeable increase in the pitting potential. With 3.5% Mo in the 18% Cr ferritic stainless steel at 25 C, the pitting potential increased in the noble direction by approximately 200 mV, while the addition of 15% of molybdenum to Fe only increased the pitting potential by approximately 100 mV.

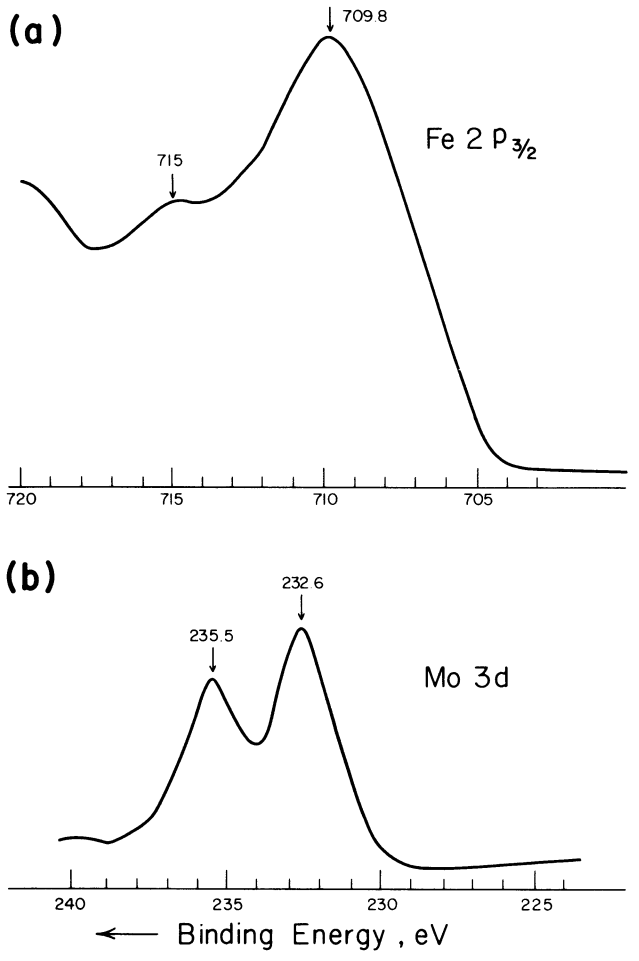

FIGURE 10 — ESCA analysis of the precipitated material.

The depletion of molybdenum observed in the passive films and unpitted areas on the 5, 10, and 15% Mo alloys resembles the situation found in stainless steels.[18] In both cases, no molybdenum was found in the surface and near surface layers, with the molybdenum increasing in the film as the substrate is approached. The absence of molybdenum in the films on these alloys is in accordance with the electrochemical results where only a small change in the passive current density was observed. Thus, Mo is not present in the near surface layers to influence the two components comprising the passive current density, *i.e.*, film dissolution and film growth. However, in the high Mo binaries where large anodic current densities were observed, Mo was present in relatively large quantities in the surface layers of the films. The corrosion product in the flow region of the primary pits can be identified using approximate quantitative analysis. This can be attempted by using Auger spectra taken from standards. Auger peak-to-peak heights can be corrected using relative elemental sensitivity factors for iron and molybdenum.[19] The use of these sensitivity factors has to be approached cautiously because of inherent uncertainties of matrix effects, surface differences, etc., but they can be a good guide to approximate concentrations in some cases. Using the sensitivity factors for iron and molybdenum for the deposited material gives

$$\frac{C_{Fe}}{C_{Mo}} \approx 1$$

where C_{Fe} and C_{Mo} are the atomic concentrations of Fe and Mo, respectively. The ESCA analysis of the deposited film indicated that iron was the +2 oxidation state and molybdenum in the +6 state. These results suggest that this corrosion product is ferrous molybdate. This is in accordance with the results of Kodama and Ambrose[20] who found that molybdate added to a borate buffer solution containing chloride inhibited the propagation of pits but not pit initiation in Fe. Molybdenum was found in the repassivated pits in the form of a $FeMoO_4$ salt. The results of this investigation suggest that the molybdate salt film found in and around pits on Fe-Mo binaries is a corrosion product, and although it likely retards pit propagation, its formation is not responsible for the increased pitting resistance derived from the presence of alloyed molybdenum. This is further supported by the absence of such a salt film in pits on Fe-17Cr-xMo ferritic stainless steels.[21]

One similarity between these results and those for the stainless steels[21] was the high chloride concentration both in the pits and in the film on the unattacked surface. Also an ESCA investigation of Fe-Mo binaries after exposure to a chloride solution showed that the chloride content of the repassivated film increased with the Mo content in the alloy.[22] Similar results were obtained for the stainless steels.[21] All of this appears to suggest that there is some type of interaction between Mo and Cl, which either forms a chemisorbed film or a salt film which has some protective properties. The observations that Mo does not affect the passive current density or the repassivation rate[23] unless chloride ions are present also supports this idea. However, this still does not explain why the addition of relatively small amounts of Mo to stainless steels can increase the pitting potential several hundred millivolts more than the addition of 15% Mo alone to iron.

Summary

1. The passive films on iron-molybdenum binaries are depleted in molybdenum.
2. As long as only a single phase is present in the alloys, increasing the molybdenum content improves the resistance to pitting, but with less effect than in stainless steels. The pitting potentials follow a similar temperature dependence as ferritic stainless steels.
3. A corrosion product, which was identified as $FeMoO_4$ was found in the primary pits and along the flow regions.
4. Molybdenum appears to form a species with chlorine which has some protective properties.

Acknowledgement

The authors would like to thank Dr. James D. Redmond and Dr. Paul Bond of the Climax Molybdenum Company for providing the binary alloys used in this study. The support of the National Science Foundation grant DMR76-20807 and the Science Center IR&D are gratefully acknowldege.

References

1. E. A. Lizlovs and A. P. Bond. J. Electrochem. Soc., Vol. 118, p. 22 (1971).
2. A. P. Bond. J. Electrochem. Soc., Vol. 120, p. 603 (1973).
3. E. A. Lizlovs and A. P. Bond. J. Electrochem. Soc., Vol. 122, p. 719 (1975).
4. E. A. Lizlovs and A. P. Bond. J. Electrochem. Soc., Vol. 122, p. 589 (1975).
5. R. F. Steigerwald, A. P. Bond, H. J. Dundas, and E. A. Lizlovs. Corrosion, Vol. 33, p. 279 (1977).
6. M. Prazak and V. C. Ihal. Corrosion Science, Vol. 2, p. 71 (1962).
7. V. Hospadaruk and J. V. Petrocelli. J. Electrochem. Soc., Vol. 113, p. 878 (1966).
8. A. P. Bond and E. A. Lizlovs. J. Electrochem. Soc., Vol. 115, p. 1130 (1968).
9. R. P. Jackson and D. Van Rooyen. Corrosion, Vol. 27, p. 203 (1971).
10. R. J. Brigham. Corrosion, Vol. 28, p. 177 (1972).
11. R. J. Brigham and E. W. Tozer. Corrosion, Vol. 29, p. 33 (1973).
12. W. P. Sykes. Tras. A.S.S.T. p. 839 (1926).
13. A. K. Sinha, R. A. Buckley, and W. Hume-Rothery. J. Iron and Steel Institute, p. 191 (1967).
14. S. Smialowska and M. Czachor. Localized Corrosion, NACE-3, p. 353 (1974).
15. C. R. Brundle, T. J. Chaung, and K. Wandelt. Surface Science, Vol. 68, p. 459-468 (1977).

16. R. Holm and S. Storp. Appl. Phys., Vol. 12, p. 101-112 (1977).
17. D. A. Stout, J. B. Lumsden, and R. W. Staehle. To be published.
18. J. B. Lumsden and R. W. Staehle. Scripta Met. Vol. 6, p. 1205 (1972).
19. Handbook of Auger Electron Spectroscopy, Second Edition (1976).
20. T. Kodama and J. R. Ambrose. Corrosion, Vol. 33, p. 5 (1977).
21. J. R. Galvele, J. B. Lumsden, and R. W. Staehle. J. Electrochem. Soc., Vol. 125, p. 1204 (1978).
22. J. R. Ambrose. Proceedings of the 4th International Symposium on Passivity, (1977).
23. J. R. Ambrose. Corrosion, Vol. 34, p. 1 (1978).

A Model for Cobalt 60/58 Deposition on Primary Coolant Piping in a Boiling Water Reactor*

W. R. DEHOLLANDER *

Abstract

A first principles model for deposition of radioactive metals into the corrosion films of primary coolant piping is proposed. It is shown that the predominant mechanism is the inclusion of the radioactive species such as Cobalt 60 into the spinel structure of the corrosion film during the act of active corrosion. This deposition can occupy only a defined fraction of the available plus 2 valence sites of the spinel. For cobalt ions, this ratio is roughly 4.6×10^{-3} of the total iron sites. Since no distinction is made between Cobalt 60, Cobalt 58, and Cobalt 59 in this process, the radioactivity associated with this inclusion is a function of the ratio of the radioactive species to the nonradioactive species in the water causing the corrosion of the pipe metal. The other controlling parameter is the corrosion rate of the pipe material. This can be a function of time, for example, and it is shown that freshly descaled metal when exposed to the cobalt containing water can incorporate as much as 10×10^{-3} cobalt ions per iron atom in the initial corrosion period. This has implications for the problem of decontaminating nuclear reactor piping. Equations and selected observations are presented without reference to any specifically identified reactor or utility, so as to protect any proprietary interests.

Opportunity exists in current BWRs to minimize or reduce the radiation fields which are present in the reactor coolant circuitry when the reactor is shut down. The major contributors to this radiation are two isotopes of cobalt, Cobalt 60 and Cobalt 58. Cobalt 58 is important in the early shutdown period, but the real isotope of concern is Cobalt 60, which is long-lived and has a substantial gamma activity. In order to control the radiation buildup, which currently averages about 100 mR per effective full power year, it is important to understand how the cobalt is deposited on the pipe surfaces. It is just as important to understand how the cobalt gets activated to Cobalt 60 and the nickel to Cobalt 58, and how these species are released from their activation sites and transported to the out-of-reactor pipe surface. However, this paper will address only the deposition of the isotope, and a separate effort is underway which will attempt to bring quantitative understanding to the activation, release, and transport mechanisms.

This paper presents a methematical model for the deposition of radioactive cobalt species on pipe walls and will *not* treat the other parts of the phenomena.

Much work has been done by many workers[1-8] in attempting to describe in mathematical terms how the radioactive atoms are deposited on out-of-reactor surfaces. Most of the approaches have been marginally successful in predicting the buildup with time for a particular reactor. In addition, work is being done by co-workers at General Electric to characterize the deposits on the piping of many reactors, by several techniques. It is to these latter workers that the author of this paper owes a great deal of credit, for their laborious efforts have provided the data base from which the present model could be formulated.

It is not appropriate to go into the chronological development of the present model. It is apparent that much additional work remains to be done to conclusively prove a total model. At General Electric in San Jose, California a good portion of this work is underway and will continue for some time.

Presentation of the Model

A word of description of the model is as follows:

The number of atoms of radioactive cobalt deposited on any area of pipe surface is directly proportional to the number of spinel iron atoms formed on that area of metal surface, multiplied by the ratio of cobalt sites to iron sites in the spinel, and the ratio of the soluble radioactive cobalt species to the soluble nonradioactive species of cobalt *in the reactor water*. The implied integration is to be carried out from the time the bare clean metal began to corrode in the cobalt containing water to the final time of interest. All three

*Presented during Corrosion/78, March, 1978, Houston, Texas.

*General Electric Company, San Jose, California.

0010-9312/79/000049/$3.00/0